International Journal of Nanomedicine

Dovepress
open access to scientific and medical research

Open Access Full Text Article

ORIGINAL RESEARCH

Dual Responsive Magnetic Drug Delivery Nanomicelles with Tumor Targeting for Enhanced Cancer Chemo/Magnetothermal Synergistic Therapy

Jianmeng Zhu[1,*], Yimin Yang[2,3,*], Jian Wang[1], Wenzhong Hong[1], Yiping Li[1], Zhen Wang[2], Kaiqiang Li[2]

[1]Clinical Laboratory of Chun'an First People's Hospital, Zhejiang Provincial People's Hospital Chun'an Branch, Hangzhou, Zhejiang, People's Republic of China; [2]Laboratory Medicine Center, Allergy Center, Department of Transfusion Medicine, Zhejiang Provincial People's Hospital (Affiliated People's Hospital), Hangzhou Medical College, Hangzhou, Zhejiang, People's Republic of China; [3]College of Pharmaceutical Sciences, Zhejiang University of Technology, Hangzhou, Zhejiang, People's Republic of China

*These authors contributed equally to this work

Correspondence: Zhen Wang; Kaiqiang Li, Laboratory Medicine Center, Allergy Center, Department of Transfusion Medicine, Zhejiang Provincial People's Hospital (Affiliated People's Hospital), Hangzhou Medical College, 158 Shangtang Road, Hangzhou, Zhejiang, 310014, People's Republic of China, Tel/Fax +86 571 8589 3270, Email wangzhen@hmc.edu.cn; likaiqiang@hmc.edu.cn

Introduction: Stimulus-responsive nanocarrier systems are promising in cancer treatment. They improve drug stability and facilitate controlled drug release. However, single-responsive nanocarriers still face insufficient tumor targeting and low efficacy.

Methods: In this study, we synthesized folate-modified DSPE-PEOz nanomicelles with PEG chains and loaded them with magnetic iron particles and doxorubicin (DOX). Folic acid (FA) was employed as a ligand to target cancer cells actively. The nanomicelles are biocompatible and acid-sensitive drug carriers. Magnetic field-responsive nanoparticles enable moderately controlled magnetothermal therapy of tumors regardless of tumor location. The pH/magnetic field dual-responsive nanomicelles shed their PEG layer in response to tumor tissue acidity and react to magnetic fields through magnetothermal effects.

Results: In vitro and in vivo experiments demonstrated that the nanomicelles could efficiently target cancer cells, release drugs in response to pH changes, and enhance drug uptake through magnetothermal effects.

Discussion: The dual-responsive magnetic nanomicelles are expected to enhance the anti-cancer efficacy of chemo/magnetothermal synergistic therapy.

Keywords: nanomicelles, synergistic therapy, stimulus-responsive, tumor targeting, Chemo/magnetothermal

Introduction

Cancer is a significant public health issue, and conventional chemotherapy medications often have poor pharmacokinetics and absorption, resulting in inferior therapeutic outcomes.[1] Stimulus-responsive nanocarrier systems offer promising potential in cancer therapy. They can enhance drug solubility and stability, selectively deliver drugs to tumor tissues, and minimize toxicity to healthy tissues. These nanocarriers can be designed to respond to various stimuli, such as changes in pH, temperature, or enzymatic activity.[2,3] Among these, pH-responsive nanocarriers are a hot topic. Researchers have developed various pH-responsive nanocarriers, including hydrogels, nanomicelles, and liposomes.[4,5] Nanomicelles are stable systems with extended circulation and safety.[6] By integrating PEG (polyethylene glycol) chains onto their surface, nanomicelles generate a hydration layer that prevents their binding to plasma proteins, enzymes, and other components, maintaining a lengthy circulation in the body.[7,8] pH-responsive nanomicelles infiltrate tumor tissues through enhanced permeability and long retention (EPR). The lower pH ruptures nanomicelles, swiftly releasing their pharmacological payload. This selective drug release mechanism improves chemotherapeutic efficacy and reduces undesirable effects.[9,10]

Received: 18 September 2023
Accepted: 6 December 2023
Published: 14 December 2023

Graphical Abstract

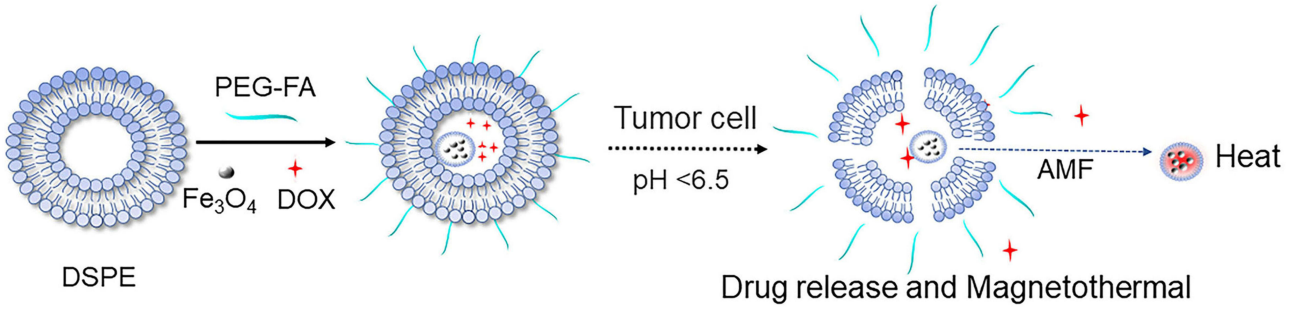

However, some limitations and challenges still need to be addressed for applying pH-responsive nanomicelles in tumor treatment. First, the pH of tumors can vary substantially between tumor types and even within the same tumor, which can lead to unpredictable drug release and poor therapeutic outcomes. Second, the EPR effect is only effective in tumors with leaky vasculature and poor lymphatic drainage and only promotes drug accumulation in the perivascular area of cancer. In contrast, the hypoxic and necrotic regions, usually found in the tumor core, remain challenging for nanocarriers to reach.[11,12]

Small-sized magnetic iron oxide nanoparticles have recently gained extensive attention in tumor therapy due to their superparamagnetic characteristics, advanced manufacturing procedures, and convenient surface modification.[13] Magnetic targeting is an emerging tumor therapy technique that involves injecting magnetic nanoparticles into the body and using an external magnetic field to deliver drugs, heat, or other therapeutic substances to the tumor tissue.[14,15] The technique can cure tumor tissue long-term and effectively with recurrent magnetic treatment. Magnetic targeting exhibits a magnetothermal effect that generates heat more uniformly than photothermal and photodynamic therapy.[16] The thermal effect is independent of tumor volume and location, allowing it to penetrate deep into the solid tumor tissue. The effect's intensity can be modulated by manipulating the magnetic field and the shape of the particles.[17] In addition, magnetothermal therapy and chemotherapy have an excellent synergistic effect. Magnetic hyperthermia can speed up drug carrier uptake by tumor cells and shorten the release time of chemotherapy drugs, avoiding cellular drug resistance and improving therapeutic outcomes.[18,19]

To further improve the tumor-targeting ability of nanomicelles, researchers have introduced various targeting molecules into nanomicelles, such as aptamers, antibodies, peptides, and ligands. Folic acid (FA), a member of the water-soluble group of vitamins, has been shown in numerous studies to be an optimal ligand for tumor targeting.[20,21] Folate receptors are highly active on the cell membranes of most human-derived malignancies (eg, ovarian, breast, cervical, colon, rectal, and nasopharyngeal cancers), and folic acid as a natural ligand for folate receptors is non-immunogenic, easily chemically bonded to other substances, and highly stable.[22,23]

In this study, we developed a pH/magnetic field dual-responsive drug-loaded nanomicelle for targeted magnetothermal synergistic chemotherapy of cancer. As Scheme 1 illustrated, we first prepared folate-modified DSPE-PEOz (DSPE-PEOz-FA, Distearoyl phosphatidylethanolamine-poly(2-ethyl-2-oxazoline)-folic acid) nanomicelles and attached PEG chains to obtain stealth nanocarriers in vivo. Then, magnetic iron particles and DOX were loaded with nanomicelles to synthesize Fe_3O_4@DOX@DSPE-PEOz-FA (DP@Fe_3O_4@DOX-FA). The magnetic nanocarriers are passively targeted by EPR and actively targeted by folic acid to reach the acidic environment of tumor tissues. At this time, the PEG layer is shed, and the nanomicelles release the drug-carrying nanoparticles, completing the first pH response and increasing the tumor cell uptake of DOX. After nanoparticles enter tumor cells, magnetic Fe_3O_4 particles encounter the magnetothermal effect caused by an external magnetic field, completing the second response. Magnetic hyperthermia raises the tumor cells' temperature and promotes drug uptake. The dual response is expected to enhance the anti-cancer efficacy by chemo/magnetothermal synergistic therapy.

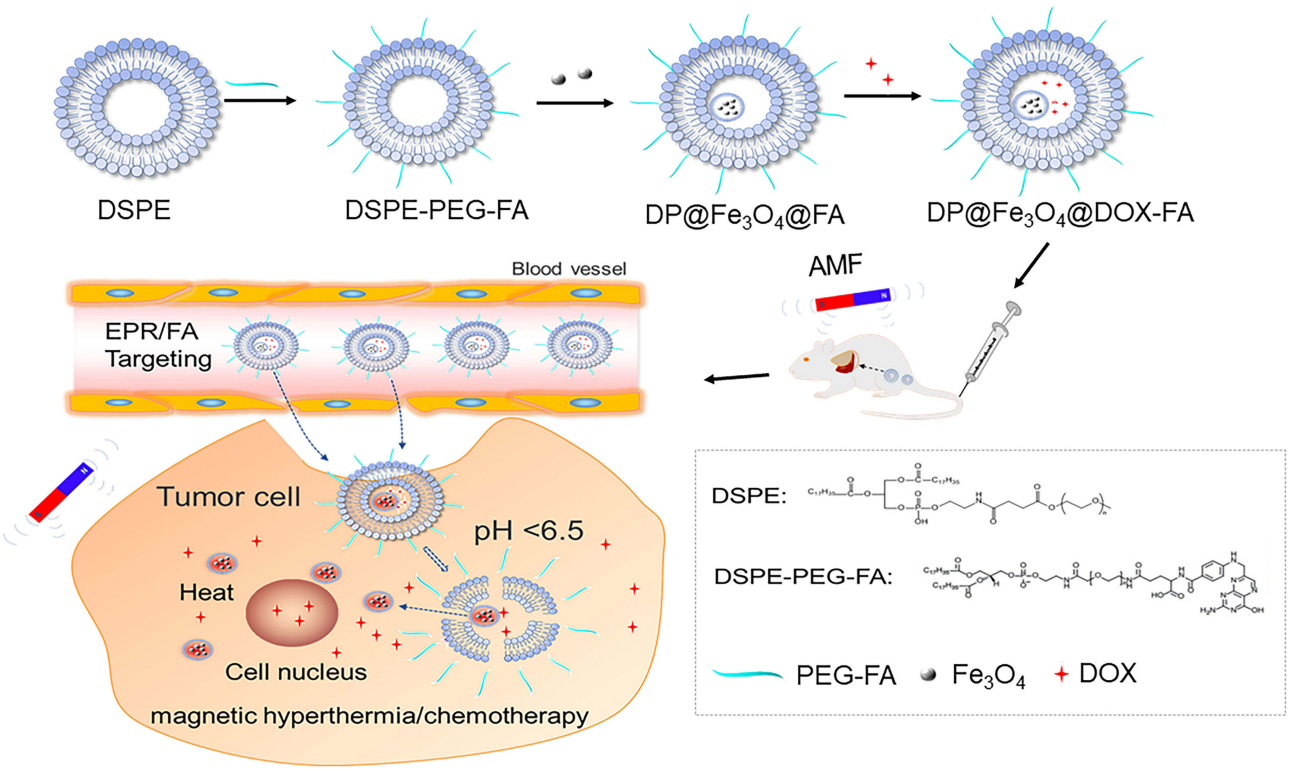

Scheme 1 Illustration of the synthesis and dual-responsive chemo/magnetothermal synergistic therapy mechanism of DP@ Fe_3O_4 @DOX-FA system. In vivo stealth nanocarriers were created by attaching PEG chains to folate-modified DSPE-PEOz nanomicelles. After loading nanomicelles with magnetic iron particles and DOX, DP@Fe_3O_4@DOX-FA was synthesized. EPR and folic acid target magnetic nanocarriers to tumor tissues' acidic environment. The PEG layer is shed, and the micelles release the drug-carrying nanoparticles, finishing the first pH response and boosting tumor cell nanomedicine uptake. The second response occurs when magnetic Fe_3O_4 nanoparticles enter tumor cells and meet the magnetothermal effect caused by an external magnetic field. Magnetic hyperthermia directly kills tumor cells and enhances chemotherapeutic intake.

Materials and Methods

Reagents

Distearoyl phosphatidylethanolamine-methyl poly(ethylene glycol) MW5000 (mPEG-DSPE) was purchased from Guangzhou Tansh Technology Co., Ltd. (Guangzhou, China). DSPE-PEOz-FA was purchased from Xi'an Ruixi Technology Co., Ltd. (Xi'an, China). DOX·HCl was purchased from Aladdin Industrial Corporation (Shanghai, China). Fe_3O_4@OA (oleate) was purchased from Nanjing Xianfeng nano Biotechnology Co., Ltd. (Nanjing, China). Chloroform was purchased from Sinopharm Chemical Reagent Co., Ltd. (Shanghai, China). All chemicals and reagents were analytical grades.

Cell Culture

Huh-7 cells were purchased from the Chinese Academy of Science Cell Bank (Shanghai, China). The cells were cultured in Dulbecco's modified Eagles medium (Gibco) and supplemented with 10% fetal bovine serum, 100 U/mL penicillin, and 100 μg/mL streptomycin in a humidified atmosphere containing 5% of CO_2 at 37°C.

Tumor-Bearing Animal Model

Female BALB/c nude mice (6–8 weeks) were provided by Jiangsu Jitaike Biopharmaceuticals Co., Ltd. (Nanjing, China). The Animal experiment protocol has been reviewed and approved by Laboratory Animal Management and Ethics Committee of Zhejiang Provincial People's Hospital. All animal experiments were conducted in accordance with the guidelines of Laboratory Animal Management and Ethics Committee of Zhejiang Provincial People's Hospital, the

guidelines followed include provisions for the welfare of laboratory animals. 1.5×10^6 Huh-7 hepatocellular carcinoma cells in the logarithmic phase were seeded into the foreleg's right axilla to establish tumor-bearing mice.

Synthesis of DP@Fe_3O_4@DOX-FA

To prepare the DOX-HCl-loaded chloroform solution, 20 mg DOX-HCl was dissolved in 5 mL water. To this, 10mL chloroform was added and shaken gently. DOX-HCl did not diffuse into the chloroform layer. Next, a 20mM $NaHCO_3$ solution was added dropwise to the solution with slight shaking until the color of DOX in the chloroform layer became brighter, and the color in the aqueous phase became purple. The resulting chloroform solution was separated and kept aside for further use. To prepare the DOX-loaded lipid nanoparticles (DP@Fe_3O_4@DOX-FA), 150 mg of DSPE-mPEG and 50 mg of DSPE-PEOz-FA were dissolved in 5 mL of the previously prepared DOX-chloroform solution. The resulting solution was then placed in an eggplant bottle, and 10mg of Fe_3O_4@OA was added. Next, 6mL of purified water was added, and the mixture was emulsified using an ultrasonic shaker. The emulsion was then evaporated for 30 minutes under rotary evaporation at 70°C water bath temperature until no further bubbles were generated, resulting in a translucent solution. Finally, the product was separated and purified using a 30k ultrafiltration tube. The materials were characterized by transmission electron microscopy (TEM, HT7800, Hitachi, Tokyo, Japan), hydrodynamic particle size analyzer (Malvern Panalytical, Zetasize LAB, Malvern, United Kingdom), Fourier infrared Spectroscopy (FTIR, LAMBDA950, Shimadzu, Japan) and UV spectrophotometer (UV-1780, Shimadzu, Kyoto, Japan).

Drug-Loading Capacity, Encapsulation Efficiency, and in vitro Drug Release of DP@Fe_3O_4@DOX-FA

An acetonitrile solution containing 10% tretinoin was prepared. Three standards of known DOX concentration and DP@Fe_3O_4@DOX-FA solution were added to the acetonitrile solution separately, and then the spectra were scanned in the UV spectrophotometer (DP@ Fe_3O_4@DOX-FA solution was diluted two-fold). Drug loading capacity (mg/mL) = Amount of DOX in nanoparticles/Volume of the solution, ie, adriamycin concentration. Encapsulation efficiency = Amount of DOX in nanoparticles/Amount of DOX input. To evaluate the drug release efficiency, drug-loaded micelles were placed at pH 6.0 or pH 7.2 with or without AMF (418 Oe, 250 kHz) application for 10 min and the supernatant was collected after incubation at room temperature for different time. UV-vis spectrophotometer (UV-1780, Shimadzu, Japan) measured DOX absorbances, and the drug release curves due to AMF and pH stimulation were plotted.

Cellular Fluorescence Detection

Laser scanning confocal microscopy (CLSM, TI-E-A1, Nikon Corporation, Tokyo, Japan) was used to observe the fluorescence of Huh-7 cells. First, Huh-7 cells were added to 35 mm four-well culture dishes and incubated for 12 h at 37°C in a CO_2 incubator; the original culture medium was removed, and 500 μL of DP@ Fe_3O_4@DOX-FA or free DOX culture medium was added and placed in a 37°C CO_2 incubator for 4 h or 2 h with or without the AMF (418 Oe, 250 kHz, 10 min); the culture medium was removed and washed with PBS for three times (2 mL/time); 1 mL of 4% paraformaldehyde solution was added and placed in a refrigerator at 4°C for 12h, and then imaging was performed. Further, the cellular uptake of DOX was measured by flow cytometry at 488 nm (Agilent, Hangzhou, China). Briefly, Huh-7 cells were inoculated in 24-well plates at a 1.0×10^5 cells/well. After 12 hours of cell culture, the cells were treated as described above. Subsequently removing the medium, cells were collected using tryptic digestion. Supernatants were then removed, and the cells were centrifuged again with 300ul stain buffer. The resulting mixture was filtered and added to flow-through tubes to detect DOX fluorescence. The data were analyzed using NovoExpress software.

Toxicity Assessment of Nanomaterials and in vitro Cell Killing Experiments

In vitro toxicity of DP@ Fe_3O_4-FA and the tumor cell killing ability of DP@ Fe_3O_4@DOX-FA were investigated by the MTT (3-(45)-dimethylthiahiazo(-z-y1)-35-di-phenytetrazoliumromide) method. Huh-7 cells in the logarithmic phase were harvested, and the culture medium was removed. For the toxicity assay, the cells were added with DP@ Fe_3O_4-FA at different concentrations of Fe_3O_4 with or without the AMF (418 Oe, 250 kHz, 10 min). For the killing assay, the

cells were treated with free DOX or DP@Fe_3O_4@DOX-FA at different concentrations of DOX with or without the AMF (418 Oe, 250 kHz, 10 min); after incubation, the culture medium was removed and washed with PBS. MTT solution was added to each well, mixed, and removed after incubation. A small amount of DMSO solution was added and shaken for 10 min to dissolve the formazan crystals. The UV spectrophotometer measured the absorbance value to determine the relative cell survival rates.

Tumor MRI Imaging

MRI images were acquired on an I-CON MR scanner (Bruker USA).100 μL PBS or DP@Fe_3O_4@DOX-FA solution (Fe concentration of 150 μg/mL) was injected via the tail vein. with or without the AMF (418 Oe, 250 kHz, 10 min). After 30 min, the mice were anesthetized with 5% chloral hydrate, and in vivo T2 MRI was performed at 24 h. The T1 cor imaging conditions were TE = 9 ms, TR = 500 ms, average number = 4, slice thickness = 1 mm, and FOV = 35 mm * 35 mm. Each experimental group was imaged twice.

In vivo Fluorescence Signal Detection

Fluorescent images of the tumor-bearing mice were obtained by an in vivo image formation system (IVIS Lumina XR III, USA). 100 μL of DOX or DP@Fe_3O_4@DOX-FA solution (Fe concentration of 150 μg/mL) was injected via the tail vein with or without the AMF (418 Oe, 250 kHz) application for 10 min per 6 h, and in vivo fluorescence imaging was performed at 480 nm excitation wavelength at 0 h, 12 h, 24 h, and 48 h.

In vivo Antitumor Efficacy Assessment

The tumor-bearing mice were divided into five groups (n = 8/group): group 1 was injected with PBS via the tail vein, group 2 received free DOX, group 3 received DP@Fe_3O_4-FA, and DP@Fe_3O_4@DOX-FA was injected into groups 4 and 5. For groups 3 and 5, the AMF(418 Oe, 250 kHz) was applicated for 10 min per 6 h. For the dosing groups, the dose of DOX was set uniformly at 6 mg/kg per group and administered every two days. Tumor volume was measured every two days during treatment. It was determined by the long and short diameter of the tumor (d, D) for tumor volume (V) ($V = d^2 \times D/2$). After 20 days of treatment, mice were euthanized according to animal welfare requirements, and tumor tissues were separated and weighed. H-E staining of tumor tissues assesses the tumor treatment of each group. To evaluate the biotoxicity of magnetic nanomicelles, tissues from major organs of PBS and DP@ Fe_3O_4@DOX-FA (AMF) groups were collected for H-E staining. Finally, survival curves were plotted based on the survival time of mice.

Statistical Analysis

Data were presented as mean ± SD. Statistically significant differences were determined using the independent samples *t*-test, and $p< 0.05$(*) was defined as statistically significant differences and highly significant differences when $p< 0.01$ (**).

Results and Discussion

Characterization

TEM was used to analyze the particle size and morphology of Fe_3O_4, DP@Fe_3O_4@DOX-FA. Figure 1a and b display TEM images of Fe_3O_4, and DP@ Fe_3O_4,@DOX-FA at pH 7.2, respectively. The average size of Fe_3O_4 particles is approximately 10 nm. Due to the comparatively high amount of magnetic particles encapsulated within the nanomicelles, their size is approximately 105 nm. Figure 1c displays TEM images of nanomicelles at pH 6.0. As shown in the figure, the increased acidity of the solution causes the nanomicelles to decompose, releasing both the medication and the magnetic particles.

DLS (Dynamic light scattering) analysis revealed that Fe_3O_4 (Figure 1d) and DP@ Fe_3O_4@DOX-FA (Figure 1e) were well distributed in solution (PDI< 0.5), with the size of approximately 32.2±1.8 nm and 133.1± 3.6 nm, respectively. Due to medium viscosity, and diffusion coefficient, hydrodynamic particle size is slightly bigger than nanoparticle size.

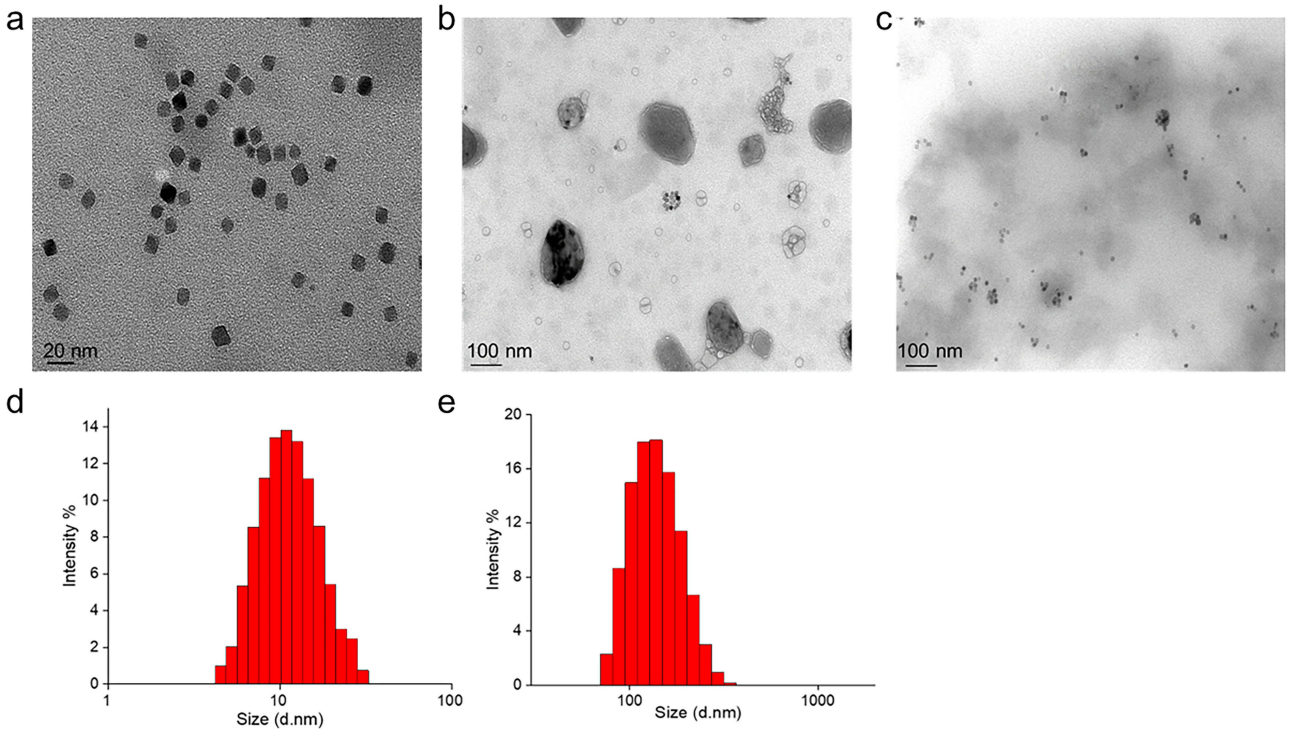

Figure 1 Nanoparticle size and morphology measurements. TEM images of Fe_3O_4 (**a**), DP@Fe_3O_4,@DOX-FA (**b**) at pH 7.2 and DP@Fe_3O_4,@DOX-FA (**c**) at pH 6.0. Hydrodynamic particle sizes measurement of Fe_3O_4 (d) and DP@Fe_3O_4,@DOX-FA (**e**). (**d**) and (**e**) were created using OriginPro 2019b software (OriginLab Corporation, Northampton, MA, USA).

The chemical functional groups of the synthesized nanomaterials were characterized by Fourier transform infrared (FTIR) spectroscopy (Figure 2). As shown in the figure, the band at 586 cm−1 corresponds to Fe-O group, and a large band at 3425 cm−1 might be caused by O-H and NH stretching vibrations in Fe_3O_4@OA. For the IR spectrum of DOX, the amino group's vibration at 3528 cm-1 disappears in the spectrum of the synthesized material, indicating the group's reaction. The peak at 3324 cm-1 relates to the vibration of the hydroxyl group on the benzene ring in DOX. 1729 cm-1 corresponds to the carbonyl group and is preserved in the spectrum of DP@Fe_3O_4@DOX-FA. The spectrum of the synthesized material shows stretching in the backbone of the aromatic ring of FA at 1465 cm-1, the C-O group in the PEG at 1114 cm-1, the amide bond vibration at 1639 cm-1, implying the amidation reaction, and the wide band at 3361 cm-1, corresponding to the OH acid groups on FA, the C-H stretching bands in DSPE's aliphatic structure match the vibrational frequency at 2918 cm-1. The above analysis shows that DSPE was effectively loaded with Fe_3O_4 particles, DOX and PEG-FA.

Assessment of Nanomicelle Drug Loading and Dual Responsive Drug Release in vitro

To calculate the drug loading capacity of the magnetic drug-loaded nanomicelles(DP@Fe_3O_4@DOX-FA), we first measured the UV absorbance values of three DOX standard solutions (Figure 3a) and then plotted a standard curve of DOX concentration versus UV absorbance values(Figure 3b). After that, we measured the nanomicelles' UV absorbance values. When FA-modified DSPE nanomicelles encapsulate adriamycin, the UV-absorbing aromatic ring structure in FA can interact with the aromatic ring structure in DOX by π-π stacking, thus affecting the UV absorption spectrum of DOX. Figure 3a shows that the nanomicelles' UV peak was red-shifted, demonstrating DOX loading. The absorption peak and DOX standard curve indicate the concentration of DOX, ie, drug loading capacity of 0.098mg/mL. To further calculate the drug encapsulation rate, we added three different concentrations of DOX standard solutions to the nanomicelles, then removed the unbound DOX and measured their absorbance values. (Figure 3b). Encapsulation efficiency = Amount of DOX in nanoparticles/Amount of DOX input. The concentration of DOX in the nanomicelles was obtained by reading the UV absorbance value, and then the encapsulation efficiency was calculated to be about 85%.

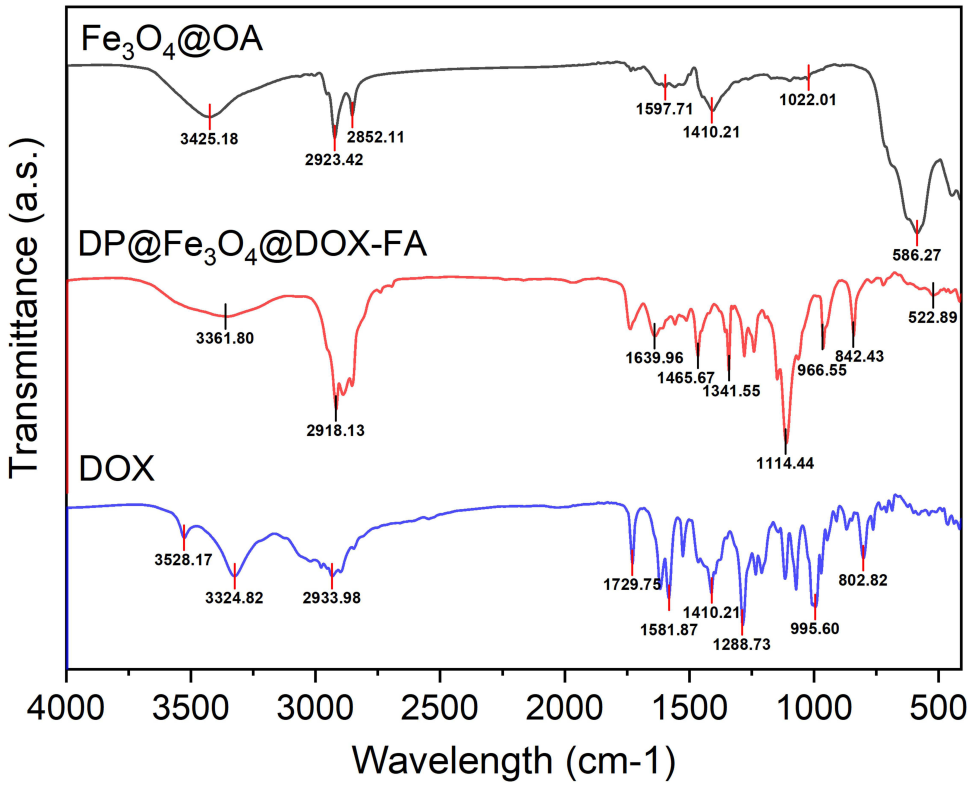

Figure 2 FTIR analysis of Fe_3O_4@OA, DP@Fe_3O_4@DOX-FA and DOX. In Fe_3O_4@OA, O-H and NH stretching vibrations may cause the broad band at 3425 cm−1 and the Fe-O group band at 586 cm−1. The amino group's 3528 cm-1 vibration disappears in DOX's IR spectrum, showing the group's reaction. DOX's hydroxyl group on the benzene ring vibrates at 3324 cm-1. DP@Fe_3O_4@DOX-FA preserves the carbonyl group at 1729 cm-1. IR of DP@Fe_3O_4@DOX-FA shows the stretching in the aromatic ring of FA at 1465 cm-1, the C-O group in the PEG at 1114 cm-1, vibration of amide bond at 1639 cm-1, indicating amidation reaction, and the wide band at 3361 cm-1 corresponding to the OH acid groups on the FA ring. DSPE's aliphatic structure has C-H stretching bands at 2918 cm-1. The graph were generated by OriginPro 2019b.

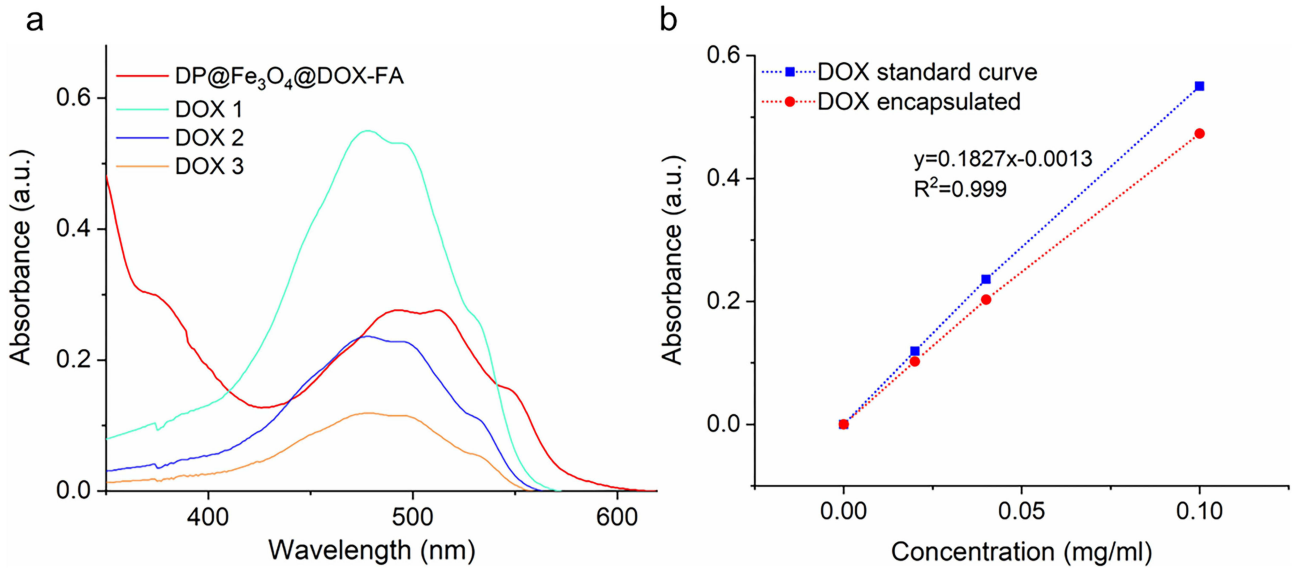

Figure 3 Measurement of Drug loading capacity and Encapsulation efficiency of DP@Fe_3O_4@DOX-FA. (**a**) UV absorbance values of three DOX standard solutions and DP@Fe_3O_4@DOX-FA. (**b**) UV absorption curves of different concentrations of DOX added to the nanomicelles and DOX encapsulated in the nanomicelles. Graphing was undertaken in OriginPro 2019b.

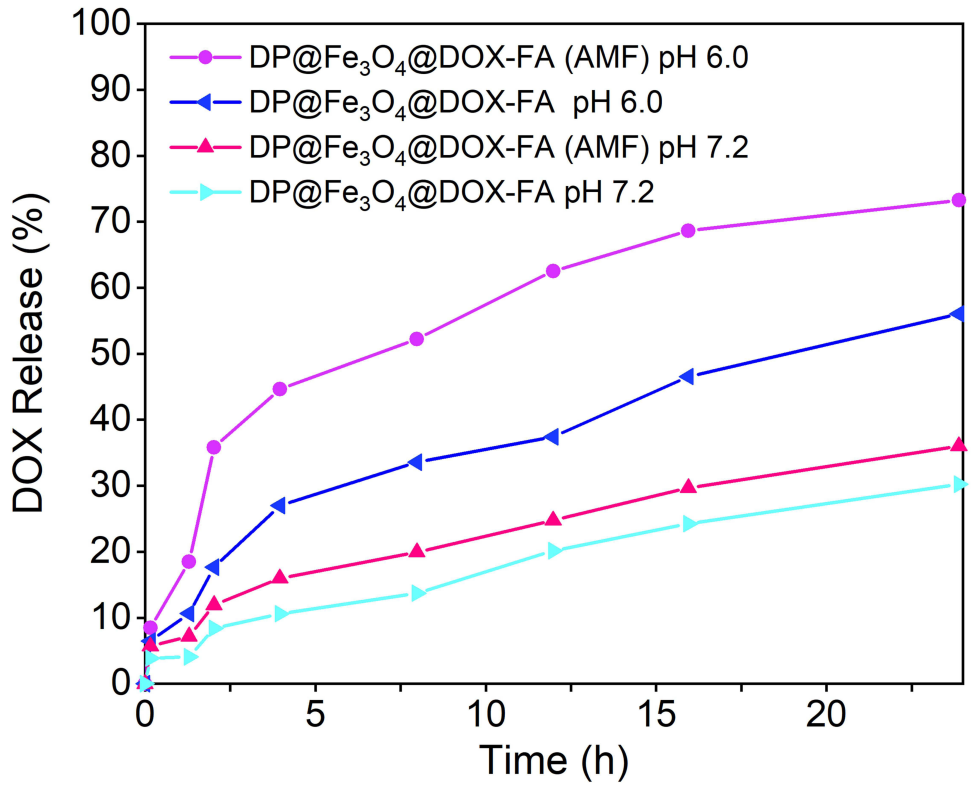

Figure 4 Drug release patterns of the nanomicelles under different stimuli. OriginPro 2019b software was used to plot the results.

Tumor cells have a pH gradient environment from early endosomes (pH 6.0–6.5) to late endosomes (pH 5.0–6.0) and then to lysosomes (pH 4.5–5.0). The nanomicelles can enter tumor cells through the endocytosis pathway and distribute in the acidic environment of endosomes and lysosomes. pH 6.0 is a representative acidic condition of tumors. To explore the drug release behavior of the nanomicelles, we evaluated their drug release efficiency at pH 6.0 and 7.2, respectively. Figure 4 shows that nanomicelles released less drug at pH 7.2 than at 6.0. The AMF improved drug release efficiency in nanomicelles at the same pH. In acidic environments where AMF is present, the nanomicelles can release more than 70% of the drugs, which suggests that a dual stimulus is much more effective at releasing drugs than a single trigger.

In vitro Cellular Targeting and Uptake

To evaluate cellular targeting and uptake of DP@Fe_3O_4@DOX-FA, the intracellular DOX fluorescence was detected with CLSM. The Huh-7 cells were incubated with DP@Fe_3O_4@DOX-FA for 2h and 4h with or without the AMF. As shown in the merged images of Figure 5, the fluorescence of the free DOX group was weaker than that of the DP@Fe_3O_4@DOX-FA (2h) group after incubation with cells for 4h. DP@Fe_3O_4@DOX-FA (AMF 2h) group has stronger fluorescence than DP@Fe_3O_4@DOX-FA groups without the AMF application. The flow cytometry measurement displays the relative frequencies of cellular uptake. The cellular internalization of free DOX exhibited a low level. In contrast, the drug-loaded nanomicelles exhibited a noticeable increase. The AMF significantly enhanced the cellular uptake of nanomicelles, leading to a notable uptake frequency of 98.6%. The photographs demonstrate that the nanomicelles targeted DOX to cells, and the AMF enhances the uptake of DOX.

In vitro Cytotoxicity Evaluation

DP@Fe_3O_4-FA includes DSPE-PEOz, FA, PEG, and Fe_3O_4. DSPE-PEOz is a phospholipid that is lipophilic and biocompatible. Folic acid is water-soluble and not biotoxic. PEG, known as polyethylene glycol, is a non-toxic, FDA-approved, non-immunogenic polymer. The toxicity of DP@Fe_3O_4-FA mainly lies in iron, so we examined its toxicity to cells at different Fe_3O_4 concentrations. Figure 6a shows that DP@Fe_3O_4-FA without DOX loading was biocompatible, as

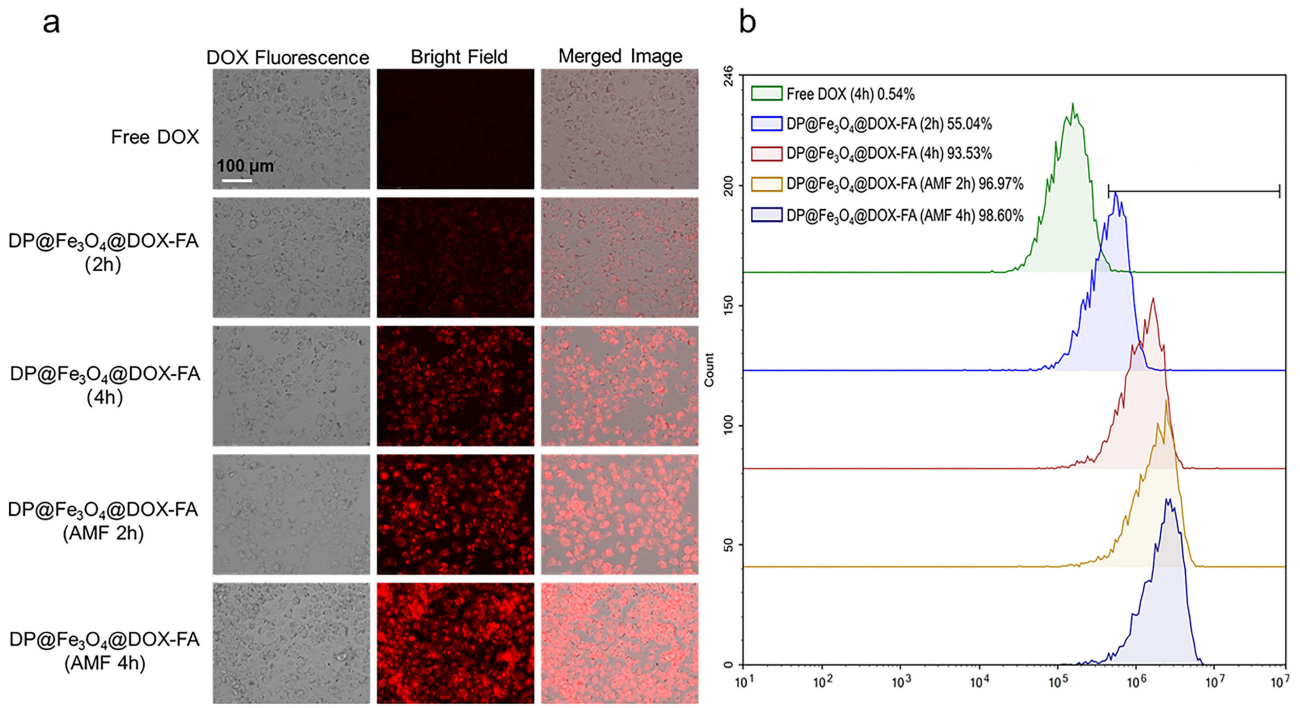

Figure 5 Cytofluorescence assay. Cellular targeting and uptake of DP@Fe_3O_4@DOX-FA and DOX were examined by CLSM (**a**) and flow cytometry (**b**).

cell survival was over 65% even at high doses (640 μg/mL). Due to the magnetothermal effect, the DP@Fe_3O_4-FA(AMF) group had lower cell survival but was still over 60%. It also indicates that the magneto-thermal effect is moderate. Figure 6b shows the tumor cell-killing statistics of DP@Fe_3O_4@DOX-FA at different DOX concentrations with or without the AMF. DP@Fe_3O_4@DOX-FA killed more tumor cells than Free DOX because it targeted tumor cells more effectively. AMF enhances the killing capacity of DP@Fe_3O_4@DOX-FA, and at a DOX concentration of 100 g/mL, it kills about 60% of tumor cells.

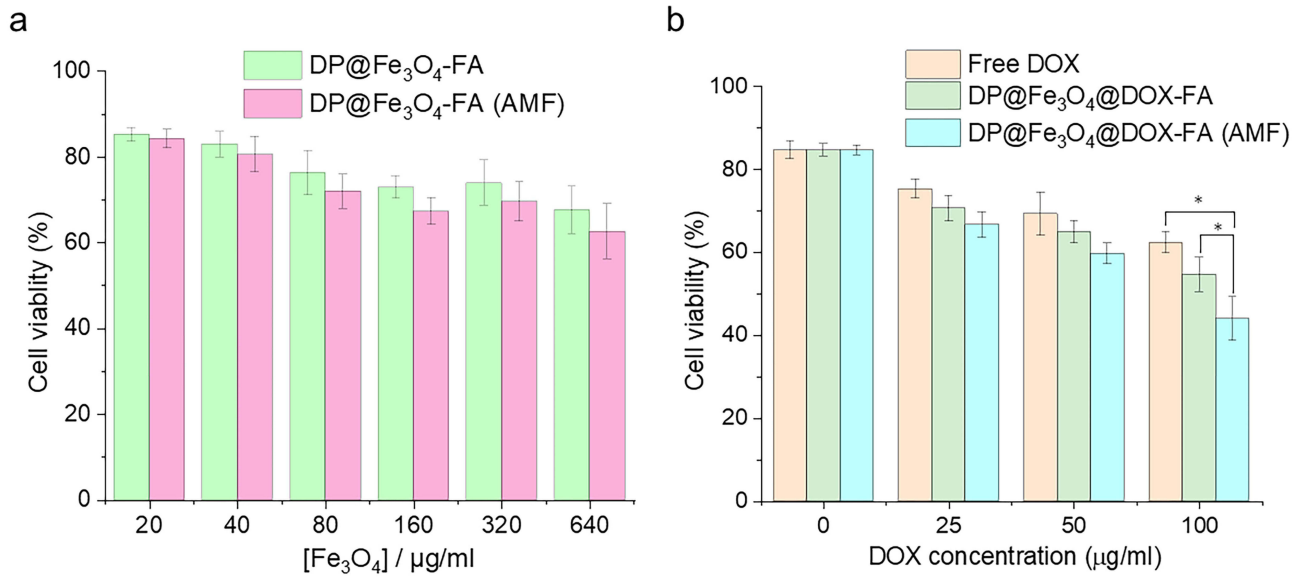

Figure 6 Statistical chart of cytotoxicity experiments. (**a**) Toxicity analysis of DP@Fe_3O_4-FA without DOX loading to tumor cells (**b**) Tumor cell killing research using free DOX and DP@Fe_3O_4@DOX-FA with or without the AMF. *$p < 0.05$. Graphs were created using OriginPro 2019b software.

Tumor MRI Signal Detection

To evaluate the magnetic properties of DP@Fe_3O_4@DOX-FA, we injected the magnetic nanomicelles into mice for tumor MRI imaging. For each experimental group, MRI imaging was performed twice. As shown in the Figure 7, nanoparticles dimmed the tumor area, and the AMF also reduced the signal value. When adding the magnetic field, the nanoparticles were activated better and produced better MRI contrast effects. The signal values of the tumor sites for each group are as follows: PBS (181.149T), DP@Fe_3O_4@DOX-FA 1(36.849T), DP@Fe_3O_4@DOX-FA 2 (37.155T), DP@Fe_3O_4@DOX-FA(AMF) 1(28.926T), DP@Fe_3O_4@DOX-FA(AMF) 2 (29.792T).

In vivo Live Imaging and Targeting

Figure 8a shows the fluorescence images of the nanomicelles (DP@Fe_3O_4@DOX-FA) after injection into the mice. Figure 8b shows the histogram of fluorescence intensity statistics. As exhibited in Figure 8a, the DP@ Fe_3O_4@DOX-FA group showed drug aggregation at the tumor site at 12h, while the DOX group did not. At 24h, a slight red fluorescence was visible in the DOX group. In contrast, the DP@Fe_3O_4@DOX-FA group and the DP@Fe_3O_4@DOX-FA(AMF) group displayed significantly enhanced red fluorescence, indicating that the nanomicelles actively targeted DOX to the tumor region, and AMF enhanced the targeting effect of DOX. At 48h, the fluorescence of experimental groups was significantly reduced because the nanomicelles were metabolized and degraded in vivo to reduce the toxic side effects.

In vivo Chemo/Magnetothermal Synergistic Therapy Evaluation

Figure 9a shows the tumor tissue images of mice at the end of the 20-day treatment. The tumor volumes of the PBS group are the largest, followed by the DOX group. The volumes of the DP@Fe_3O_4@-FA (AMF) group are larger than

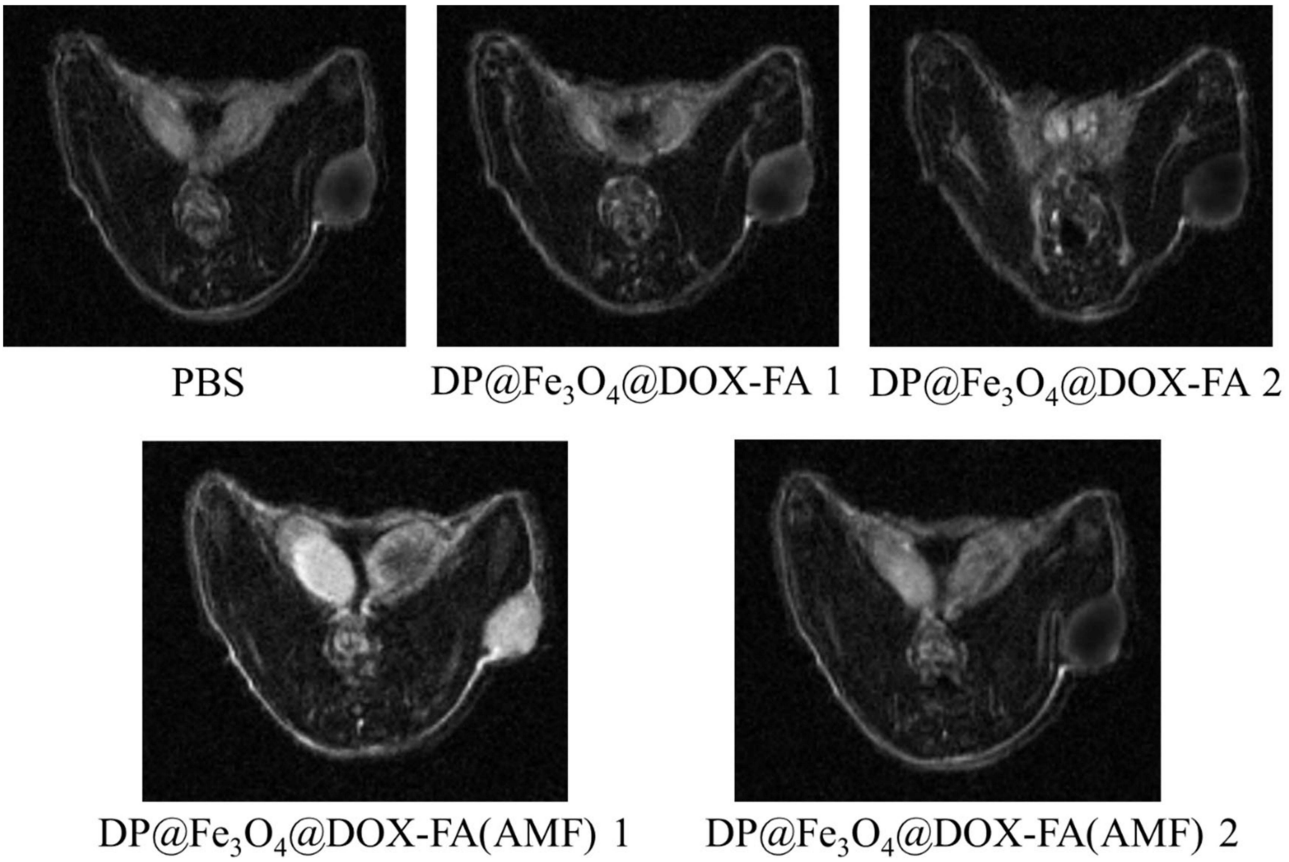

Figure 7 MRI imaging of tumors with DP@Fe_3O_4@DOX-FA with or without the AMF.

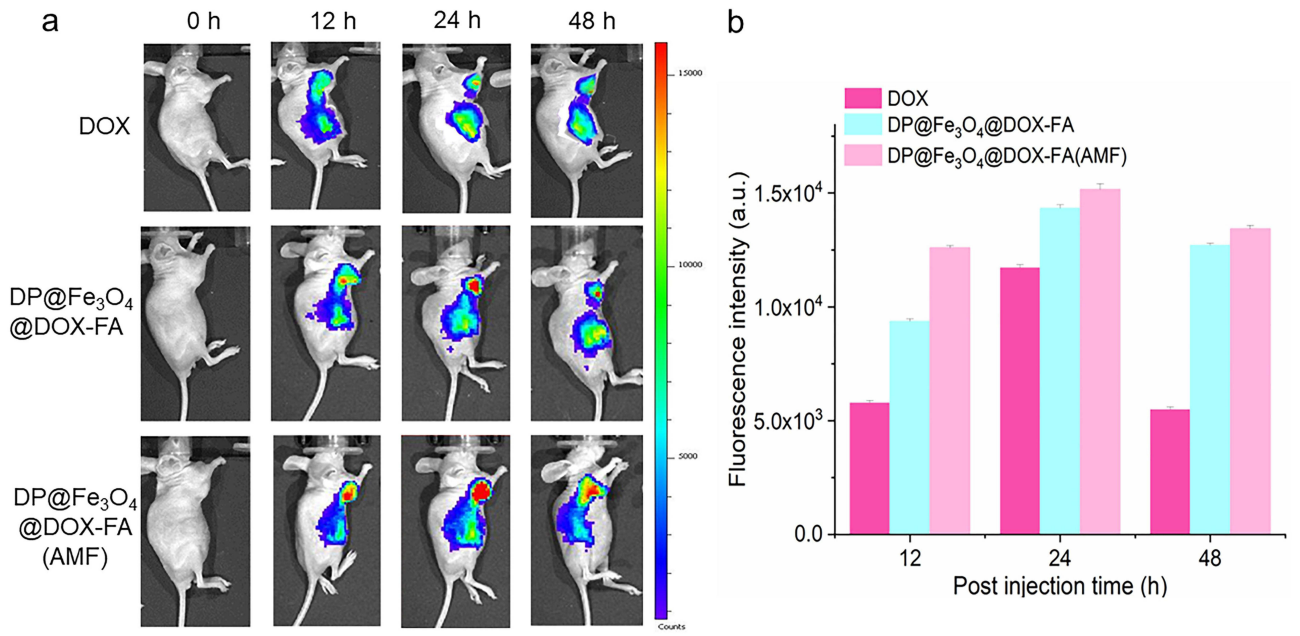

Figure 8 In vivo targeting and drug uptake. (**a**) Distribution of free DOX and the nanomicelles with or without the AMF after injection into mice. (**b**) Histogram of fluorescence intensity statistics (created using OriginPro 2019b software).

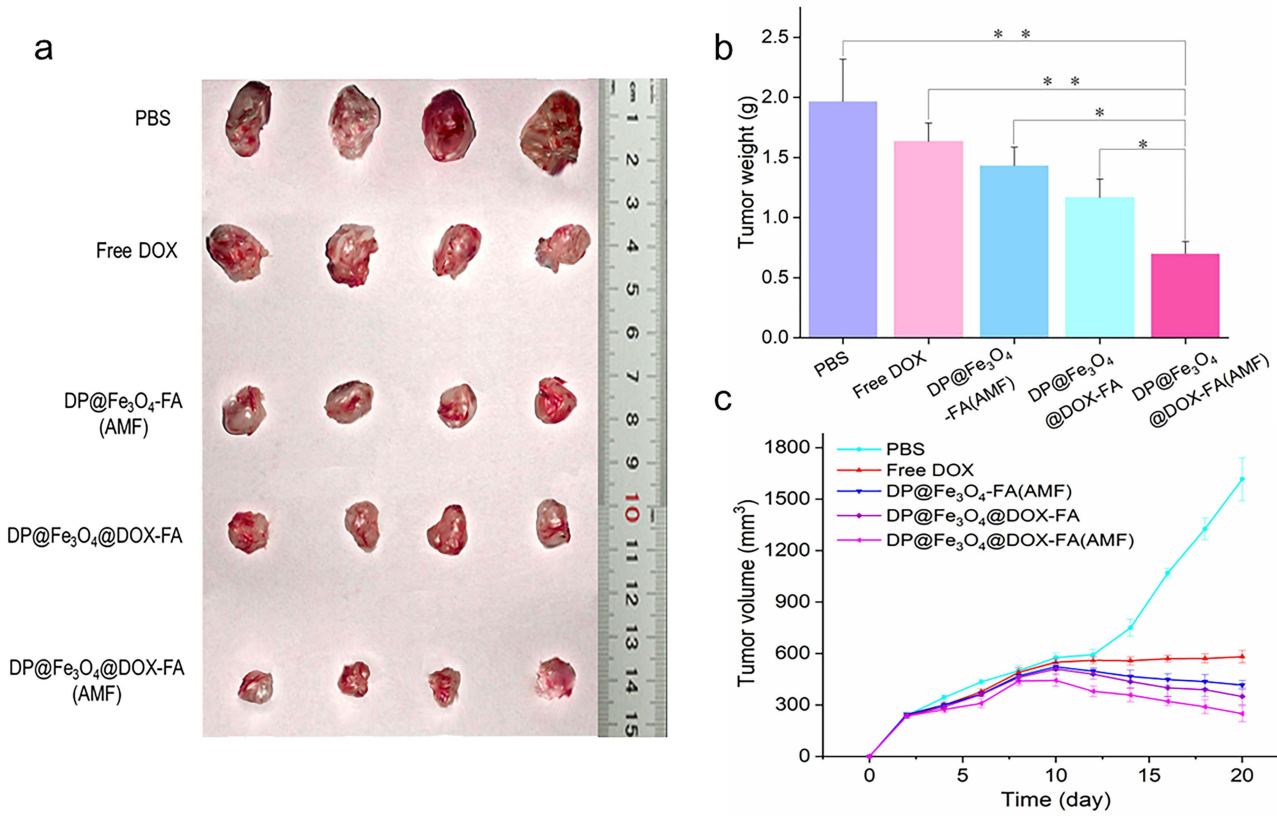

Figure 9 Antitumor effectiveness in vivo. (**a**) The tumor tissue images of mice after 20 days of therapy (**b**) Tumor weight statistics (**c**) Alterations in tumor volume throughout treatment. (**b**) and (**c**) were created using OriginPro 2019b software. *$p < 0.05$, **$p < 0.01$.

that of the DP@Fe_3O_4@DOX-FA group, indicating that in terms of a single treatment, the chemotherapy is more effective than the magnetothermal therapy. The DP@Fe_3O_4@DOX-FA(AMF) group shows the smallest tumor volume, which verifies that chemo/magnetothermal synergistic therapy could improve the antitumor efficacy. Figure 9b shows the tumor weight statistics of each group, and the results coincide with Figure 9a. The tumor weight of the DP@Fe_3O_4@DOX-FA(AMF) group was smaller than the other groups.

Figure 9c shows the changes in tumor volume during the treatment. On day 8, the tumor volumes were closest between the groups. After day 10, the tumor volumes of the PBS group grew fast, probably because the immune system of mice hardly suppressed tumor growth. The tumor volumes of the DOX group were nearly unchanged due to the in vivo drug resistance resulting from the low targeting. However, the other three experimental groups could inhibit tumor growth, and the DP@Fe_3O_4@DOX-FA(AMF) group showed the smallest tumor volumes at the end of treatment. HE staining was performed to assess the toxicity of DP@Fe_3O_4@DOX-FA to the major organs of mice and tumor tissue after treatment. Figure 10a shows the HE staining images of tumor tissues at the end of treatment in each group of mice. Tumor cell nuclei in the PBS and DOX groups almost covered the field of view but were seldom found in the DP@Fe_3O_4@DOX-FA(AMF) group. Therefore, its anti-tumor efficacy was better than that of single therapy groups, ie, DP@Fe_3O_4@DOX (AMF) and DP@Fe_3O_4@DOX-FA. As shown in Figure 10b, no significant damage was found in the heart, liver, spleen, lung, and kidney of the DP@Fe_3O_4@DOX-FA(AMF) group, indicating the drug-loaded nanomicelles system were biocompatible. Figure 11 presents the survival curves of mice. Kaplan-Meier curves indicate the median survival times for the PBS, Free DOX, DP@Fe_3O_4@-FA(AMF), DP@Fe_3O_4@DOX-FA, and DP@Fe_3O_4@DOX-FA(AMF) groups were 33, 36, 43, 50, and 70 days, respectively. This result demonstrates that dual-responsive drug-loaded nanomicelles can effectively synergize chemotherapy and magneto-thermal therapy to improve tumor treatment.

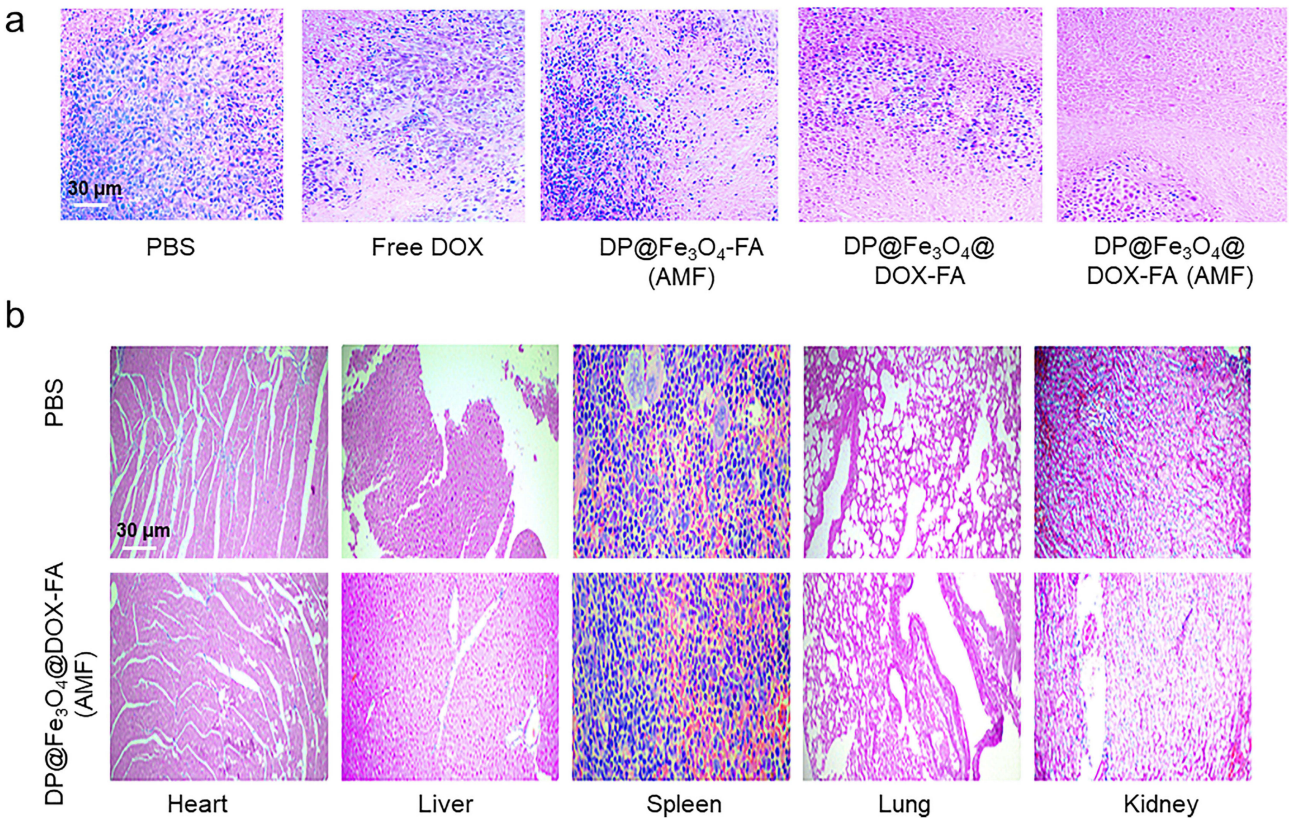

Figure 10 HE-stained images (**a**) Tumor tissues after different treatments. (**b**) Assess the toxicity of DP@Fe_3O_4@DOX-FA with the AMF to the major organs.

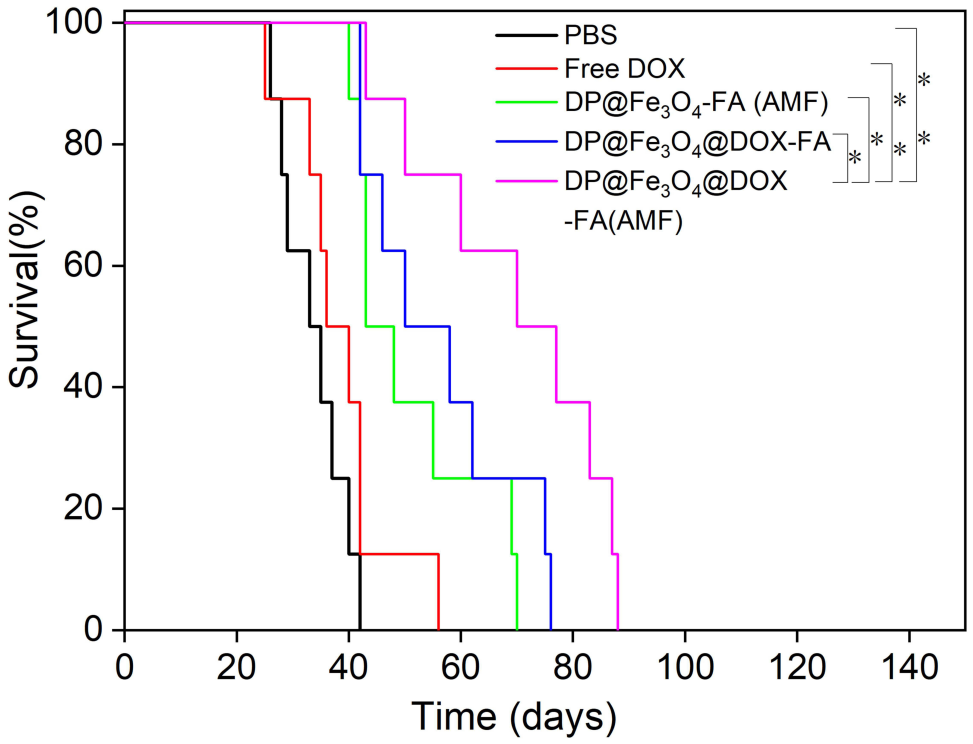

Figure 11 Survival analysis of mice in each group (created using OriginPro 2019b software). *$p < 0.05$, **$p < 0.01$.

Conclusions

This study has developed and characterized dual-responsive magnetic drug delivery nanomicelles (DP@Fe_3O_4@DOX-FA). These nanomicelles possess the EPR effect, active folic acid targeting, and magnetic targeting. Selective drug release and tailored magnetothermal therapy for cancer have been rendered possible by the nanomicelles' sensitivity to pH and magnetic fields. The dual-responsive magnetic drug delivery nanomicelles with tumor targeting showed significantly enhanced treatment efficacy than traditional chemotherapy and mono-responsive nanomicelles. The approach provides a promising strategy for enhanced chemo/magnetothermal synergistic therapy. Cellular and animal experiments did not reveal any noticeable biotoxicity of the nanomicelles. Additionally, efforts should be made to optimize the design of these nanocarriers to increase their targeting efficiency and safety. The successful translation of these nanocarriers to clinical use could significantly enhance cancer treatment outcomes and improve patients' quality of life.

Acknowledgments

This research was supported by Traditional Chinese Medicine Scientific Research Project of Zhejiang Province (2023ZL010) and Zhejiang Medical and Health Science and Technology Project (2021KY272, 2022KY529).

Disclosure

The authors declare no competing interests in this work.

References

1. Saha RN, Vasanthakumar S, Bende G, Snehalatha M. Nanoparticulate drug delivery systems for cancer chemotherapy. *Mol Membr Biol*. 2010;27(7):215–231. doi:10.3109/09687688.2010.510804
2. Zhang ZT, Huang-Fu MY, Xu WH, Han M. Stimulus-responsive nanoscale delivery systems triggered by the enzymes in the tumor microenvironment. *Eur J Pharm Biopharm*. 2019;137:122–130. doi:10.1016/j.ejpb.2019.02.009
3. Pourmadadi M, Ahmadi MJ, Dinani HS, Ajalli N, Dorkoosh F. Theranostic applications of stimulus-responsive systems based on Fe(2)O(3). *Pharm Nanotechnol*. 2022;10(2):90–112. doi:10.2174/2211738510666220210105113

4. He Y, Fan X, Wu X, et al. pH-Responsive size-shrinkable mesoporous silica-based nanocarriers for improving tumor penetration and therapeutic efficacy. *Nanoscale*. 2022;14(4):1271–1284. doi:10.1039/D1NR07513F
5. Zhang WJ, Li S, Vijayan V, et al. ROS- and pH-responsive polydopamine functionalized Ti(3)C(2)T(x) MXene-based nanoparticles as drug delivery nanocarriers with high antibacterial activity. *Nanomaterials*. 2022;12(24):4392. doi:10.3390/nano12244392
6. Yu YM, Bu FZ, Yu Y, et al. 5-fluorouracil-caffeic acid cocrystal delivery agent with long-term and synergistic high-performance antitumor effects. *Nanomedicine*. 2022;17(30):2215–2229. doi:10.2217/nnm-2022-0208
7. Yi T, Qian J, Ye Y, et al. Crizotinib nanomicelles synergize with chemotherapy through inducing proteasomal degradation of Mutp53 proteins. *ACS Appl Mater Interfaces*. 2023;15(1):511–523. doi:10.1021/acsami.2c18020
8. Yao L, Daniels J, Wijesinghe D, Andreev OA, Reshetnyak YK. pHLIP(R)-mediated delivery of PEGylated liposomes to cancer cells. *J Control Release*. 2013;167(3):228–237. doi:10.1016/j.jconrel.2013.01.037
9. Du T, Wang Y, Luan Z, Zhao C, Yang K. Tumor-associated macrophage membrane-camouflaged pH-responsive polymeric micelles for combined cancer chemotherapy-sensitized immunotherapy. *Int J Pharm*. 2022;624(121911):121911. doi:10.1016/j.ijpharm.2022.121911
10. Gao Y, Zhou Y, Zhao L, et al. Enhanced antitumor efficacy by cyclic RGDyK-conjugated and paclitaxel-loaded pH-responsive polymeric micelles. *Acta Biomater*. 2015;23:127–135. doi:10.1016/j.actbio.2015.05.021
11. Koo AN, Lee HJ, Kim SE, et al. Disulfide-cross-linked PEG-poly(amino acid)s copolymer micelles for glutathione-mediated intracellular drug delivery. *Chem Commun*. 2008;48(48):6570–6572. doi:10.1039/b815918a
12. Piktel E, Niemirowicz K, Watek M, et al. Recent insights in nanotechnology-based drugs and formulations designed for effective anti-cancer therapy. *J Nanobiotechnol*. 2016;14(1):39. doi:10.1186/s12951-016-0193-x
13. Cheng HW, Tsao HY, Chiang CS, Chen SY. Advances in magnetic nanoparticle-mediated cancer immune-theranostics. *Adv Healthc Mater*. 2021;10(1):e2001451. doi:10.1002/adhm.202001451
14. Abed Z, Shakeri-Zadeh A, Eyvazzadeh N. Magnetic targeting of magneto-plasmonic nanoparticles and their effects on temperature profile of NIR laser irradiated to CT26 tumor in BALB/C mice. *J Biomed Phys Eng*. 2021;11(3):281–288. doi:10.31661/jbpe.v0i0.1032
15. Chen S, Song Y, Yan X, et al. Injectable magnetic montmorillonite colloidal gel for the postoperative treatment of hepatocellular carcinoma. *J Nanobiotechnol*. 2022;20(1):381. doi:10.1186/s12951-022-01559-7
16. Zhao S, Yu X, Qian Y, Chen W, Shen J. Multifunctional magnetic iron oxide nanoparticles: an advanced platform for cancer theranostics. *Theranostics*. 2020;10(14):6278–6309. doi:10.7150/thno.42564
17. Tong S, Quinto CA, Zhang L, Mohindra P, Bao G. Size-dependent heating of magnetic iron oxide nanoparticles. *ACS Nano*. 2017;11(7):6808–6816. doi:10.1021/acsnano.7b01762
18. Gavilan H, Avugadda SK, Fernandez-Cabada T, et al. Magnetic nanoparticles and clusters for magnetic hyperthermia: optimizing their heat performance and developing combinatorial therapies to tackle cancer. *Chem Soc Rev*. 2021;50(20):11614–11667. doi:10.1039/d1cs00427a
19. Wang J, Zhang W, Xie Z, et al. Magnetic nanodroplets for enhanced deep penetration of solid tumors and simultaneous magnetothermal-sensitized immunotherapy against tumor proliferation and metastasis. *Adv Healthc Mater*. 2022;11(23):e2201399. doi:10.1002/adhm.202201399
20. Donadoni E, Siani P, Frigerio G, Di Valentin C. Multi-scale modeling of folic acid-functionalized TiO(2) nanoparticles for active targeting of tumor cells. *Nanoscale*. 2022;14(33):12099–12116. doi:10.1039/D2NR02603A
21. Moharil P, Wan Z, Pardeshi A, et al. Engineering a folic acid-decorated ultrasmall gemcitabine nanocarrier for breast cancer therapy: dual targeting of tumor cells and tumor-associated macrophages. *Acta Pharm Sin B*. 2022;12(3):1148–1162. doi:10.1016/j.apsb.2021.09.024
22. Wang X, Wei W, Zheng D, Chen Z, Dai H. Folic acid-functionalized L-cys/ZnS:O nanoparticles for homologous targeting and photodynamic therapy of tumor cells. *J Mater Chem B*. 2022;10(31):6001–6008. doi:10.1039/D2TB00719C
23. Jaiswal N, Halder S, Mahata N, Chanda N. Bi-functional gold nanorod-protein conjugates with biomimetic BSA@Folic acid corona for improved tumor targeting and intracellular delivery of therapeutic proteins in colon cancer 3D spheroids. *ACS Appl Bio Mater*. 2022;5(4):1476–1488. doi:10.1021/acsabm.1c01216